Development of an optical-resolution photoacoustic microscope

Author: Jordi Torres Durall
Facultat de Física, Universitat de Barcelona, Diagonal 645, 08028 Barcelona, Spain.

Advisor: Martí Duocastella Solà

Abstract: High-resolution, non-invasive, deep imaging in highly dispersive media is a key challenge in modern microscopy, as it would lead to many biomedical advancements. A potential solution is to use the photoacoustic effect, which allows to retrieve optical information through acoustic waves. These waves are generated by the local temperature rise at the sample points irradiated with pulsed light and then propagate though the medium, experiencing much less dispersion than light. In this study, we present the development process of a custom-made optical-resolution photoacoustic microscope. To this end, we first characterized the used laser beam and optical system and found the beam width at the focus to be $w_0 \sim 40\,\mu$m. Then, we processed and analyzed the photoacoustic signal, detected with a transducer, using the Hilbert transform. Finally, we show that images can be retrieved successfully from a sample using the designed and assembled microscope. We anticipate that the proposed OR-PAM microscope is a first step toward the use of the photoacoustic effect for deep imaging at micrometric resolution, and could be further improved and optimized by using a lower pulse energy and a higher sampling frequency.

I. INTRODUCTION

One of the most important challenges in modern imaging is to obtain non-invasive, high-resolution information from biological tissue or other highly dispersive media. A promising solution is to exploit the photoacoustic effect (PA), as the scattering length for acoustic waves is usually orders of magnitude higher than that for light. For instance, in human skin, the optical scattering coefficient at $\lambda = 700\,$nm is $\sim 10\,\text{mm}^{-1}$, three orders of magnitude higher than for ultrasonic waves at $f = 5\,$MHz, $\sim 10^{-3}\,\text{mm}^{-1}$. Consequently, this effect can be used to retrieve optical information from the medium at equal or higher depths than other widespread microscopy methods, such as Confocal microscopy or Two-photon microscopy. Furthermore, it could also be used in conjunction with wavefront engineering technologies, increasing even more the depth at which information can be retrieved.[1][2]

The photoacoustic effect, also known as optoacoustic effect, occurs when a short-pulsed light is absorbed by the sample, increasing the temperature at the irradiated point. If the pulse is short enough (typically $t < 100\,$ns), thermal and stress relaxation are too slow to dissipate the heat and a pressure increase is created. Therefore, the absorbed energy is dissipated by emitting a wideband acoustic pulse that can be detected using an ultrasonic transducer.[3]

PA has many applications and is a fast-growing research topic, specially in biomedical optics. One of its most studied implementations is Photoacoustic Tomography (PAT), which enables a computerized 2D or 3D reconstruction of the scanned tissue. The main branches of this technique are Optical Resolution PAM (OR-PAM, up to $\sim 1.5\,$mm depth), Acoustic Resolution PAM (AR-PAM, up to $\sim 5\,$mm depth) and Photoacoustic Computed Tomography (PACT up to $\sim 7\,$cm depth). Both OR-PAM and AR-PAM are based on the scanning of the sample, their main difference being what defines its resolution: OR-PAM relies on ballistic photons and a tight laser focusing, while AR-PAM depends on a smaller acoustic focus. On the other hand, PACT operates using an unfocused light source and a transducer array to detect the absorption position.[1][3]

Additionally, PAT presents a big advantage over other biologic tissue imaging methods, as it allows to use a high variety of both endogenous and exogenous contrast agents. Examples of widely used endogenous contrast agents in PAM are hemoglobin for vascular imaging in the IR range and DNA for cellular imaging in the UV range. Meanwhile, exogenous contrast agents can be used to increase molecular sensitivity, as in the case of nanoparticles, or even to achieve superresolution in the case of fluorophores.[3]

This study is focused on OR-PAM, as it has the best lateral resolution between the different discussed PAT systems. We first present a brief theoretical explanation of the effect and then describe the process of creating a custom-made OR-PAM microscope; including the design, the process of laser characterization, the acoustic signal treatment and a proof of its imaging capabilities.

II. PRINCIPLES

A. Ultrasound wave generation

The acoustic wave generated in the photoacoustic effect is usually created by a temperature rise in the region where the laser is absorbed. The equations that describe temperature diffusion and acoustic wave propagation in a medium are given by (Eq. 1), and their characteristic relaxation time scales in the illuminated region can be approximated using (Eq. 2):[3]

$$\left(\nabla^2 - \tfrac{1}{\alpha}\tfrac{\partial}{\partial t}\right) T = 0, \qquad \left(\nabla^2 - \frac{1}{v_s^2}\frac{\partial^2}{\partial t^2}\right) p = 0, \quad (1)$$

$$\tau_{th} = \tfrac{d_c^2}{\alpha_{th}}, \qquad \tau_s = \frac{d_c}{v_s}. \quad (2)$$

Where d_c is the width of the region, α_{th} is the thermal diffusivity and v_s is the speed of sound in the medium.

If the laser pulse is short enough to assume thermal and stress confinement ($\tau < \tau_s, \tau_{th}$), the fractional volume change of the region is negligible, and the absorbed energy leads to a local temperature increase that can be associated with a pressure increase:

$$\frac{\Delta V_0}{V} = -\kappa \Delta p_0 + \beta \Delta T_0 \approx 0, \tag{3}$$

$$\Delta T_0 = \eta_{th} \frac{A_e}{\rho C_v}, \qquad \Delta p_0 = \frac{\beta \Delta T_0}{\kappa}. \tag{4}$$

Where η_{th} is the fraction of absorbed light converted into heat, A_e is the specific optical energy deposition, ρ is the medium density, C_v is the specific heat capacity, β is the thermal coefficient of volume expansion and κ is the isothermal expansion coefficient.

In the case of a thin enough sample ($\mu_a x \ll 1$), and using the Beer-Lambert law, $A_e = \frac{F}{x}(1 - e^{-\mu_a x}) \approx \mu_a F$, where μ_a is the optical absorption coefficient and F is the local optical fluence. When analyzing a sample, we can assume most of the presented material and medium parameters to be approximately constant and measurable, and the generated pressure increase at each point in the sample depends on the absorption coefficient at that location. $\Delta p_0 \propto \mu_a$.[3]

The described local temperature and pressure increase leads to the formation of an acoustic wave, that follows the wave equation:

$$\left(\nabla^2 - \frac{1}{v_s^2}\frac{\partial^2}{\partial t^2}\right) p(\vec{r}, t) = -\frac{\beta}{\kappa v_s^2}\frac{\partial^2 T(\vec{r}, t)}{\partial t^2}. \tag{5}$$

In some cases, other mechanisms independent of a temperature increase can also generate a photoacoustic signal. These mechanisms are often related to photochemical reactions like photosynthesis, which produce volume changes or gas flux variations that result in acoustic wave generation under the effects of a pulsed laser.[4]

In conclusion, by measuring the pressure of the ultrasound wave using a transducer, local information from the sample can be obtained at a resolution that only depends on the laser spot size.

B. Ultrasound wave detection

A piezoelectric transducer or a transducer array are usually used to detect the acoustic wave generated by the photoacoustic effect. The configuration and shape of the transducer present great variability in order to adapt to the desired specifications and operation mode.[5]

Piezoelectric materials have the property of changing their polarization when deformed, creating an electric field in the piezoelectric effect. Consequently, piezoelectric transducers work by generating a measurable electric potential difference in the presence of an acoustic signal, which creates a non-static deformation.[6]

Therefore, the obtained signal contains information about the position of the absorption point in the transducer's axis, as a difference in axial position corresponds to a measurable delay in the time at which the pressure wave reaches the transducer ($v_s = \frac{\Delta x}{\Delta t}$). This effect is used to create PACT systems using a transducer array, or even to reduce the number of dimensions to be scanned in AR-PAM or OR-PAM microscopes. It needs to be noted that in the case of OR-PAM, the axial resolution is much lower than the lateral resolution, as the magnitude of the first depends fundamentally on the focus width and the second on acoustic wave emission and detection.[7]

III. DEVELOPMENT OF AN OR-PAM MICROSCOPE

A. Design and assembly

To produce and measure the photoacoustic effect, we used a UV laser "Flare NX 343-0.2-2 Laser Head Rev2" ($\lambda = 343\,\text{nm}$) and a piezoelectric transducer "Ultran Group, WS50-1" ($f_{res} = 1\,\text{MHz}$), submerged in water to enhance the acoustic signal. We chose an off-axis alignment configuration for the laser beam and the transducer (Fig. 1), used in some OR-PAM microscopes found in the literature [5]. In the optical system, we used a quartz aspherical lens with focal distance 7 cm and several mirrors. Additionally, we made use of a pre-existing assembly consisting of two Glan-Taylor prisms acting as linear polarizers with a half-wave plate between them to adjust the laser's power.

On a first phase, we made the scanning of the sample using manually micrometer-controlled stages and saved the data using an oscilloscope. When imaging precision was required, we automatized the movement of the sample using computer-controlled stages ("MTM 150 CC1, Newport", controlled with "ESP301, Newport") and saved the signal data using a data acquisition card ("PCI digitizer board CS23G8 CobraMax, GaGe Applied").

B. Laser Characterization

To characterize the laser beam, we studied the energy of each pulse as a function of the angle of the half-wave plate. To this end, we measured the energy for each angle using a photodetector at the end of the optical system and fitted the results applying the Malus law to the assembly. We added a minimum energy constant to take into account possible system imperfections (Fig. 2.A),

$$E = E_0 \cdot cos^2[2 \cdot (\theta - \theta_0)] + E_{min}. \tag{6}$$

We used *Microsoft Excel* to obtain a linear fit of the results, taking the value $\theta_0 = 27.7°$ that provided a better fitting. The obtained fits were $E_0 = 78.33 \pm 0.15\,\mu\text{J}$ and $E_{min} = 0.21 \pm 0.06\,\mu\text{J}$ with $R^2 = 0.9998$.

To study the laser beam size near the focus, we used a titanium thin film as a sample and selected an adequate pulse energy to produce ablation. For big enough

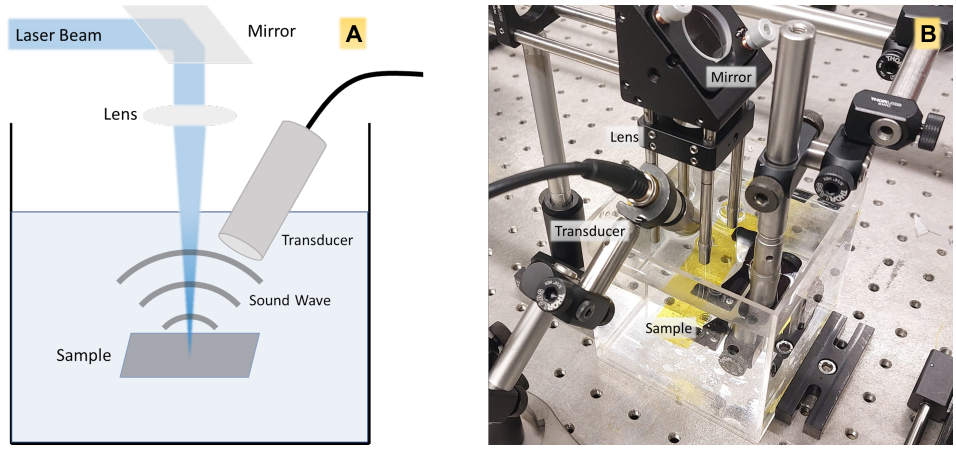

FIG. 1. Schematic design of the assembly (A) and photographic illustration of the mounted microscope (B).

energies and a Gaussian beam, we can assume the ablated region width to be proportional to the beam radius [8]. Therefore, we created a series of ablation lines using different sample heights to find the focus position and analyzed the pulse width (Fig. 2.C). We studied these lines using an optical microscope to acquire known-scale images from the sample. Then, we measured their width at several positions using *Inkscape*. Using $E = 5.6\,\mu$J, the experimental pulse width at the focus was $w_0 = 38.7 \pm 0.9\,\mu$m. We present two adjustments in the results (Fig. 2.D). Fit A is according to the width of a Gaussian beam, including quality-factor (M^2) corrections:[9]

$$w_A = w_0 \cdot \sqrt{1 + \left(\frac{z - z_0}{M^2 \cdot z_R}\right)^2}, \qquad z_R = \frac{\pi w_0^2}{\lambda}. \quad (7)$$

Fit B is a linear fit, assuming $w_B = A|z - z_0| + w_0$, and shows a higher accordance with the data. The obtained adjustments are in each case:

$$\begin{aligned} w_A(\mu\text{m}) &= (42.6 \pm 1.4) \cdot \sqrt{1 + \left(\frac{z(\text{mm})}{3.1 \pm 0.2}\right)^2}, \\ w_B(\mu\text{m}) &= (6.8 \pm 0.2) z(\text{mm}) + (38.6 \pm 0.4), \\ \text{with} \quad & R_A^2 = 0.94 \quad \text{and} \quad R_B^2 = 0.998. \end{aligned}$$

In both cases, the data collected further away from the focus has not been included to calculate the adjustments because the optical fluence is lower in this region, and we cannot assume the ablated width to be proportional to the beam radius. In particular, the theoretical fit (Fit A) may fail to correctly adjust the data due to spherical aberration (produced by the water interface), poor beam shape, formation of bubbles due to ablation, mechanical vibrations or pulse energy instabilities.

We used a camera to measure the intensity distribution of the beam (Fig. 2.C) and found it not to be as Gaussian as expected ($M^2 = 1.01$ in the laser's specifications). The observed imperfections in the distribution could be caused by dust adhesion on any of the optical components of the assembly or on the camera's filter, as dust absorbs in the UV wavelength used in the experiment (343 nm). Although a Gaussian beam allows a tighter focusing, it should be noted that other beam distributions could be better suited for an OR-PAM system. For instance, a top-hat beam, with a uniform intensity distribution, would allow a better, more homogeneous sampling in each scanned point.

The described characterization was a necessary development step, as it allowed to estimate the beam width to be $w_0 \sim 40\,\mu$m, which sets the lateral resolution of the microscope. Meanwhile, the conducted experiments were not dependent on axial resolution, as the used samples were very thin flat surfaces.

C. Acoustic signal processing

The signal $f(t)$ generated by the transducer when detecting a photoacoustic wave presents oscillations that can make it difficult to measure a robust scalar value to assign to each scanned point. Therefore, it is usually characterized using the Hilbert transform $\mathcal{H}$, which allows to calculate the analytic signal $S(t)$ and then its instantaneous amplitude $A(t)$ (Fig. 3), widely used for AR-PAM signal analysis [7]. To finally obtain a scalar value I, we numerically integrated this last magnitude. We can easily compute and interpret the Hilbert transform through its relation with the Fourier transform: positive frequency values are phase-shifted by $-\pi/2$ and negative frequency values are phase-shifted by $\pi/2$. These relations are described by:[10]

$$H(t) = \mathcal{H}\{f(t)\} = \frac{1}{\pi} \int_{-\infty}^{+\infty} \frac{f(\tau)}{t - \tau} d\tau, \quad (8)$$

$$H(t) = \mathcal{F}^{-1}\{-i\, sgn(w) \cdot \mathcal{F}\{f(t)\}(w)\}, \quad (9)$$

$$S(t) = f(t) + iH(t), \qquad A(t) = |S(t)|, \quad (10)$$

$$I = \int_{t_i}^{t_f} A(t) dt. \quad (11)$$

We applied Eq. 9, 10 and 11 in succession to assign a scalar value to the measured signal at each position. For this purpose, we used *Scipy*, a *Python* library with many functionalities including signal processing functions.

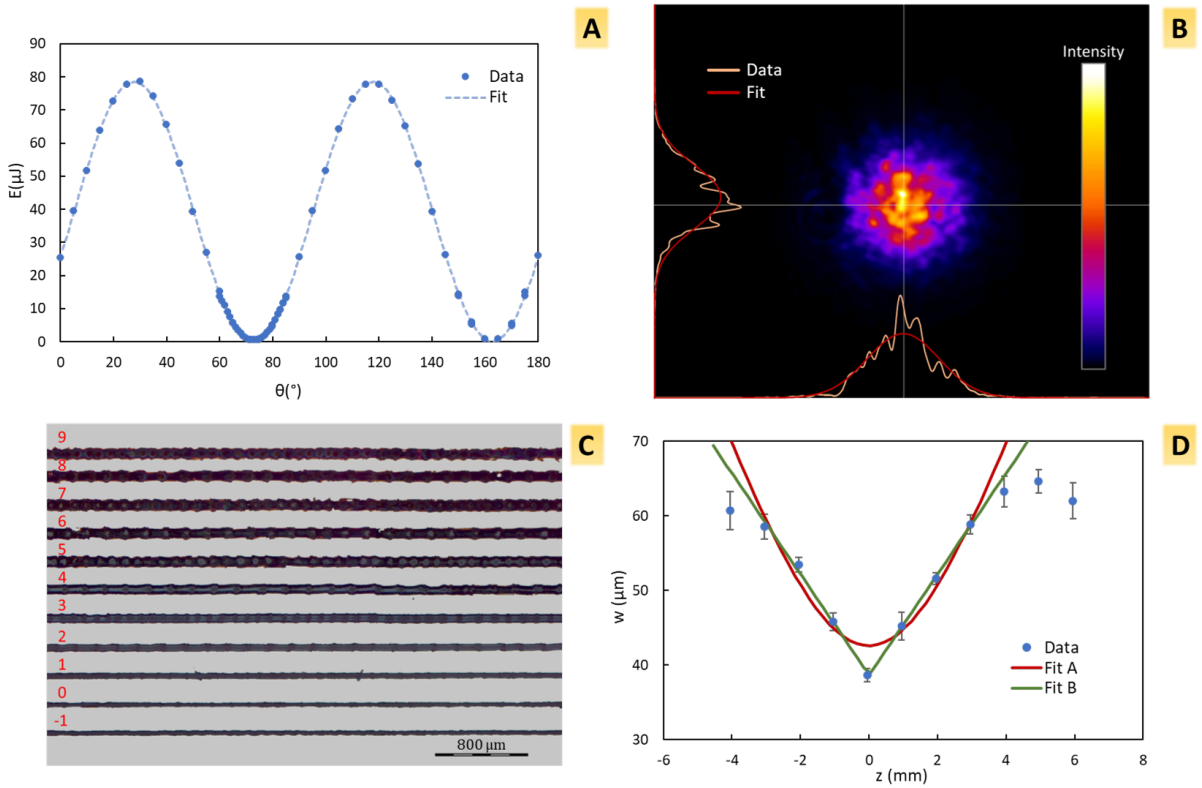

FIG. 2. Energy of each pulse as a function of the half-waveplate angle (A), pulse intensity distribution (B), ablation lines for different sample vertical positions relative to the focus, shown in mm (C), ablation line width as a function of the vertical position relative to the focus (D).

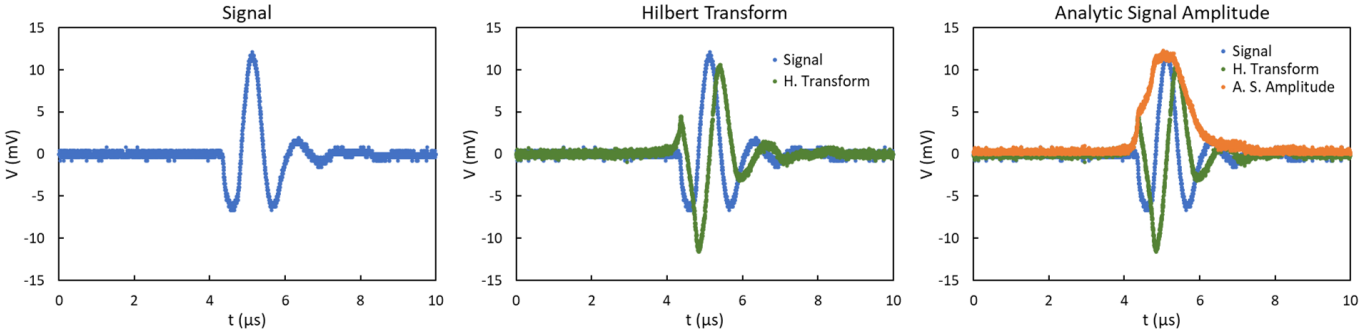

FIG. 3. Detected signal, Hilbert transform of the signal and Amplitude of the analytic signal. The presented signal was obtained when ablating a titanium thin film with $E = 5.6\,\mu$J and $w \sim 40\,\mu$m.

D. Imaging

To generate images from a sample, we automated the movement of the stages and the data acquisition using a preexisting *Labview* program. Firstly, we cut a Kapton polyimide film sample using *CorelDraw* and a preexisting custom laser printing setup controlled with *BoxDMC.exe*, to create a test image (Fig. 4.A). Then, we scanned the sample and recorded the signal produced at each point. Finally, we processed the time-dependent signal for each point using *Python* as described previously to assign a value to each point. To do this process, we adjusted the pulse energy to obtain a good signal while not generating a photoacoustic signal from the glass sample holder placed below the Kapton film, also trying not to produce big damage to the sample. For these reasons and taking into account the previous laser analysis, we used an energy $E = 14.6\,\mu$J and made scanning steps of $\Delta x = w \sim 40\,\mu$m. Although taking into account the beam width, the optimal sampling step should have been lower to maximize the acquired information [11], $\Delta x \sim 10\mu$m, this would have significantly increased the scanning time, making the imaging process too slow.

The laser beam scanning slightly damaged the sample material (Fig. 4.B). As a constant frequency was used for the laser and the stages had a limited scanning velocity, we used a very low scanning frequency (2 Hz) to avoid any unmeasured and sample-damaging laser pulses that might affect the results. These limitations resulted in a big scanning time (29 min for the 65×53 px).

We processed the resulting image (Fig. 4.C) using *Fiji* with a suitable threshold and then applied a median filter using *Python* with a proper value to eliminate iso-

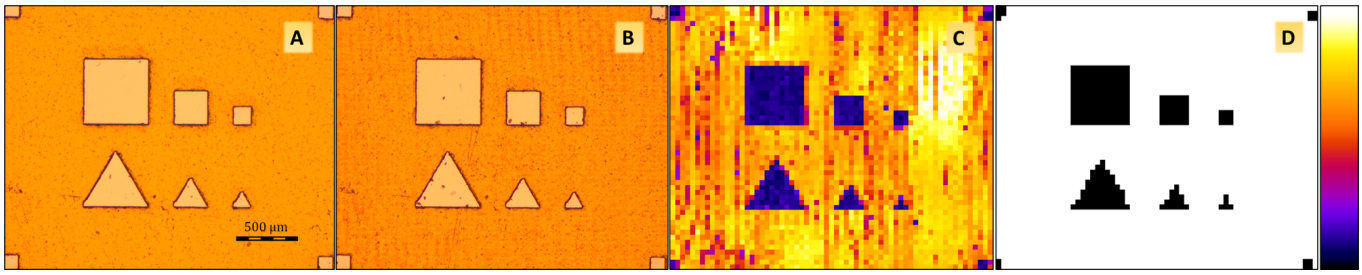

FIG. 4. Kapton film sample (over glass) before (A) and after (B) the laser scanning to induce the photoacoustic signal. Image obtained from the signal processing, normalized with the maximum value of $49.2 \cdot 10^{-6}$ V·s (C) and filtered and thresholded image (D). The used lookup table color gradient is also shown.

lated noise points. A final black and white image was obtained this way (Fig. 4.D), which accurately represented the sample image.

We found different causes as possible sources of noise in the untreated image, such as water surface vibrations when moving the sample, bubbles on the sample's surface, and specially dust particles moving on the water's interface, which could have obstructed the laser beam. We could solve many of these problems, as well as the damage made to the sample, by using a lower pulse energy to prevent sample damage and a higher pulse frequency to allow multiple measures at each point, as well as a lower scanning time. These configuration improvements would lead to a non-damaging, faster and more accurate OR-PAM microscope that could be used to retrieve information from dispersive media, such as those described in the literature.

IV. CONCLUSIONS

As our results demonstrate and in accordance with the presented theory, the photoacoustic effect can be used to retrieve optical information from a sample, with a resolution that only depends on the laser beam width in the case of OR-PAM.

The developed OR-PAM system enables micrometric imaging of samples, and can successfully create images with a resolution of $\Delta x \sim 40\,\mu$m from a Kapton film and glass sample by scanning it with a laser beam and processing the obtained acoustic signal using the Hilbert transform.

The proposed OR-PAM microscope could be improved by using a lower pulse energy and a higher sampling frequency, allowing non-destructive and faster imaging with less noise and even enabling deep imaging in dispersive media. Other potential improvements would be avoiding dust adhesion in the optical system to increase the resolution, or using a top-hat beam to make more uniform measurements at each scanned point.

ACKNOWLEDGMENTS

Foremost, I want to thank Prof. M. Duocastella for his guidance and vision and Ms. B. Mestre for her help and supervision at the laboratory. I also want to express my gratitude towards Dr. M. Colom, Mr. E. Martí, Dr. P. Ricci and Dr. A. Marchese for their patience and support throughout the project. Special thanks to prof. J. M. Hernandez for his kindness and insights about the experimental system. Finally, thanks to my partner and colleagues for their help and support while writing and formatting this work.

[1] L. V. Wang and J. Yao, *Practical guide to photoacoustic tomography in the life sciences*, Nature Methods **13**, 627 (2016).
[2] J. Yao and L. V. Wang, *Photoacoustic microscopy*, Laser & Photonics Reviews **7**, 758 (2013).
[3] Y. Zhou, J. Yao, and L. V. Wang, *Tutorial on photoacoustic tomography*, Journal of Biomedical Optics **21**, 061007 (2016).
[4] S. Malkin and O. Canaani, *The Use and Characteristics of the Photoacoustic Method in the Study of Photosynthesis*, Annual Review of Plant Physiology and Plant Molecular Biology **45**, 493 (1994).
[5] S. Jeon et al. *Development and Application of Piezoelectric Materials for Ultrasound Generation and Detection*, Photoacoustics **15**, 100141 (2019).
[6] A. Manbachi and R. S. C. Cobbold, *Review on practical photoacoustic microscopy*, Ultrasound **19**, 187 (2011).
[7] R. Cao et al. *Optical-resolution photoacoustic microscopy with a needle-shaped beam*, Nature Photonics **17**, 89 (2023).
[8] A. Žemaitis et al. *Advanced laser scanning for highly-efficient ablation and ultrafast surface structuring: experiment and model*, Scientific Reports *8*, 17376 (2018).
[9] A. E. Siegman, *How to (Maybe) Measure Laser Beam Quality* in DPSS Lasers: Applications and Issues, edited by M. Dowley, OSA Trends in Optics and Photonics Vol. 17, paper MQ1 (United States, Washington D.C., 1998).
[10] E. A. Arcos and R. E. Castillo, *The Hilbert Transform*, Surveys in Mathematics and its Applications **16**, 149 (2021).
[11] P. Vesely, *Handbook of Biological Confocal Microscopy* (Springer Science & Business Media, New York 2006, 3rd. ed.)